Heat Transfer to a Particle in a Laminar, Thermal Boundary Layer

Aaron M. Lattanzi^a, Xiaolong Yin^b, Christine M. Hrenya^{a*}
^aUniversity of Colorado at Boulder, Dept. of Chemical and Biological Engineering, Boulder, CO, USA
^bColorado School of Mines, Petroleum Engineering, Golden, CO, USA
*corresponding author

Abstract

In many industrial systems, bounding walls or immersed surfaces are utilized as the primary thermal source to heat a gas-solids mixture. As a result, the heat transfer in the near-wall region is of great significance. To resolve the heat transfer near a boundary, convection correlations developed for unbounded systems (no walls) are extended into the near-wall region in conjunction with particle-scale theories for indirect conduction. Here we rigorously test the unbounded convection correlations and indirect conduction theory against outputs from direct numerical simulation of laminar flow past a hot plate and a static, cold particle. The unbounded convection correlations alone are found to under-predict the heat transfer occurring in the near-wall region. While further incorporation of indirect conduction captures the first-order physics associated with near-wall heat transfer enhancement, the conductive length scale commonly employed for indirect conduction is incorrectly identified as being proportional to the particle size. By contrast, it is observed that the key length scale associated with near-wall heat transfer enhancement is the thickness of the wall thermal boundary layer. An approximation of the thermal boundary layer thickness from classic boundary layer theory is utilized to develop a Nusselt correlation for the near-wall region. The new correlation accounts for convection as well as indirect conduction and asymptotically decays to the unbounded convection correlation for large particle-wall separation distances, thereby seaming together the unbounded and near-wall regions.

Introduction

The design and operation of various industrial processes is highly dependent upon the transport of thermal energy within a gas-solids flow. In many systems, domain walls or immersed surfaces are utilized as the primary energy source to heat a particle-laden mixture [1-13]. Under such conditions, the heat transfer occurring between a wall and a gas-solids flow is of primary significance. Despite prevalent use of such flows in industry, fundamental explorations on wall-to-particle heat transfer have been largely unreported in the literature. While a variety of convective heat transfer correlations have been reported for unbounded gas-solids flows (no walls) [14-17], they inherently do not account for boundary effects. By and large, these unbounded correlations are applied as is to the near-wall region, where their validity is expected to deteriorate. On many occasions, direct numerical simulation (DNS) has been employed to probe the heat transfer occurring within an unbounded gas-solids system [14,16,18-26]. However, works-to-date which account for wall-to-particle heat transfer (boundary effects) are far less inclusive [9,27].

The heat transfer occurring between a particle and a wall is comprised of convective, conductive, and radiative mechanisms. For the case of moderate system temperatures (T < 700K), radiation is often neglected since it is not a significant contribution to the overall heat transfer [28-29]. Under these circumstances, the relevant heat transfer mechanisms may be simplified to convection and conduction only. Typically, correlations for unbounded systems [14-17] are utilized to approximate the interphase convection in the near-wall region. To account for conduction, particle-scale theories have been largely relied upon. Specifically, the conduction occurring between a particle and wall is made up of two contributions: (i) direct conduction

through the particle-wall contact area [30-31] and (ii) indirect conduction between a particle and wall separated by a thin layer of fluid [32]. In many practical cases, indirect conduction tends to dominate over direct conduction - i.e., when the ratio of thermal resistances associated with direct and indirect conduction is much greater than unity, or $\beta = R_p k_a \hat{h}_{PFW}(0)/2k_p R_c \gg 1$, where R_p is the particle radius, k_g is the gas thermal conductivity, $\hat{h}_{PFW}(0)$ is the solution to the indirect conduction integral at a particle-wall separation distance of zero [33], R_c is the radius of contact between the particle and wall, and k_p is the particle thermal conductivity. While particle-scale theories for indirect conduction [32,34-36] have been applied to a wide variety of systems [7-8,37-40], the theories themselves have not been validated. Most commonly, indirect conduction theory assumes that each particle is surrounded by a static fluid lens (R_{Lens}) , as denoted by the dashed line in Figure 1. When the fluid lens overlaps with the wall, one-dimensional conduction is assumed to occur through the fluid lens. Therefore, the fluid lens thickness is the key length scale that establishes distances over which particle-wall conduction will occur. Indirect conduction theory has been shown to be most sensitive to the fluid lens thickness parameter, which is traditionally set according to the particle size $(R_{Lens} \propto R_p)$ [33]. The current state-of-the-art for modeling near-wall heat transfer involves using the unbounded heat transfer correlations in the near-wall region with modifications based on particle-scale theories (indirect conduction), which have not been rigorously tested. For gas-solids flows at moderate temperatures (dominated by convection and indirect conduction), further work is required to assess the accuracy of these methods in the near-wall region.

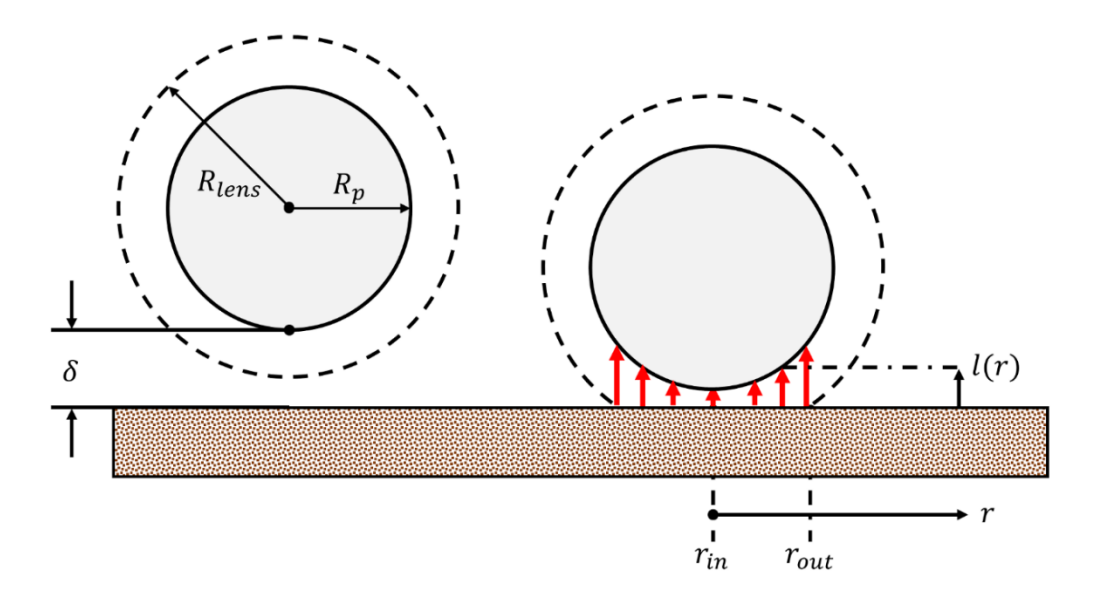


Figure 1: (left particle) An illustration of the static fluid lens (dashed line) theory employed by indirect conduction theory. (right particle) The heat transfer occurring between a particle and wall when the lens overlaps with a wall - i.e., the particle-wall separation distance (δ) is less than the fluid lens thickness ($R_{Lens} - R_p$).

In the present work, we utilize a hybrid lattice Boltzmann - random walk particle tracking (LBM - RWPT) based DNS code [41-44] to examine the heat transfer to a spherical particle in the near-wall region. The heat transfer to a static particle in a laminar, thermal boundary layer is

considered here - i.e., uniform flow of a fluid past a hot plate and a static, cold particle. The presence of a hot wall in this work allows boundary effects on wall-to-particle heat transfer to be quantified. Particle heat rates obtained from LBM-RWPT are compared to the heat rates predicted by unbounded convection [14] and indirect conduction [32] closures commonly employed within the discrete element method (DEM) framework. The unbounded convection correlations alone are found to under predict the heat transfer to a particle in the near-wall region since they do not fundamentally account for the presence of the wall. By contrast, the combination of unbounded convection and indirect conduction considerably improves agreement with LBM-RWPT. Specifically, indirect conduction theory is observed to capture the first order physics associated with heat transfer enhancement in the near-wall region. However, heat transfer enhancement is observed in LBM-RWPT at particle-wall separation distances (δ) not predicted by indirect conduction theory. Namely, indirect conduction theory sets the fluid lens thickness according to geometric arguments based upon the particle size $(R_{Lens} = 1.4R_p)$ [7-8,33-34], and thus predicts near-wall heat transfer will occur when the fluid lens intersects the wall ($\delta \leq 0.4R_n$). However, setting the fluid lens thickness in this manner neglects the thermal length scale associated with the fluid near the wall (boundary layer thickness). By contrast, we find that the thermal boundary layer thickness (δ_T) associated with the wall is the correct length scale associated with heat transfer enhancement in the near-wall region. An approximation for δ_T [45-46] is utilized to develop a Nusselt number correlation in terms of the dimensionless separation distance ($\hat{\delta} = \delta/\delta_T$). The Nusselt correlation is observed to asymptotically decay to the unbounded convection correlation in the limit of large $\hat{\delta}$ (particle outside the thermal boundary layer), and thus, seams together the unbounded and near-wall regions. Furthermore, the developed correlation accounts for heat transfer to a particle due to both convection as well as indirect particle-fluid-wall conduction.

Background: Indirect Conduction Theory

To account for the indirect conduction occurring between a particle and wall, we employ the theory proposed by Rong and Horio [8,32]. In this theory, particles are assumed to be surrounded by a static fluid lens (dashed line in Fig. 1). When the lens overlaps with the wall, one-dimensional conduction through the fluid lens is assumed to occur between the particle and wall. Motivation for describing the fluid lens as "static" is guided by the effect of no-slip boundary conditions on the particle and wall. As the separation distance (δ) between the particle and wall becomes small, the fluid velocities between the particle and wall are dramatically reduced from the free-stream velocity. The rate of heat transfer due to indirect conduction is found by integrating Fourier's law over the area of overlap between the fluid lens and wall [8]:

$$\dot{q}_{PFW} \equiv h_{pfw} \left[T_w - T_p \right] = \int_{r_{in}}^{r_{out}} \frac{2\pi k_g r}{Max(l,s)} \left[T_w - T_p \right] dr$$

$$r_{in} = \begin{cases} r_s = \sqrt{R_p^2 - \left(s - R_p - \delta \right)^2} & \delta \le s \\ 0 & \delta > s \end{cases}$$

$$r_{out} = \begin{cases} \sqrt{R_{lens}^2 - \left(R_p + \delta \right)^2} & \delta > \sqrt{R_{lens}^2 - R_p^2} - R_p \\ R_p & \delta \le \sqrt{R_{lens}^2 - R_p^2} - R_p \end{cases}$$

where \dot{q}_{PFW} is the rate of heat transfer due to indirect conduction between the wall and particle, h_{pfw} is the particle-fluid-wall heat transfer coefficient, T_w is the wall temperature, T_p is the particle temperature, r is the radial position of the fluid lens overlap, l(r) is the conduction distance at a radial position of r, s is the minimum conduction distance, δ is the particle-wall separation distance, and R_{lens} is the fluid lens radius. To evaluate the integral in Eq. 1, a fluid lens radius (R_{lens}) and minimum conduction distance (s) must be specified. An upper bound for R_{lens} is generally determined from geometric arguments and is given by $R_{lens} = \sqrt{2}R_p \approx 1.41R_p$. Namely, the maximum fluid lens radius is set such that the upper bound of integration in Eq. 1 (r_{out}) does not exceed the particle radius at the point of solid body contact $(\delta = 0)$ – i.e., the conduction distance (l) remains well defined. The fluid lens radius utilized in this work matches that commonly employed in other works $(R_{lens} = 1.4R_p)$ [7-8,33-34,37]. The minimum conduction distance (s) in Eq. 1 acts as a lower bound for the conduction distance (l). The minimum conduction distance can be physically interpreted as corresponding to either the size of surface asperities (roughness) or the mean free path of the gas (perfectly smooth particles). For the former case, large-scale asperities on the surface of a particle or wall will result in finite separation distances even at contact. For the latter case, as the particle and wall tend to solid body contact $(\delta = 0)$, the conduction distance (l(r)) becomes small with respect to the mean free path of the gas and rarefaction effects become non-negligible. By setting the minimum conduction distance to the mean free path of the gas (air at STP) $(2.75 \times 10^{-8} \text{ m})$, the integration in Eq. 1 avoids conduction lengths where rarefaction effects are significant. Here, the particle and wall will be assumed to be perfectly smooth and the range of separation distances (δ) considered will be larger than the mean free path of the gas. Therefore, the lower bound of integration in Eq. 1 (r_{in}) will always be 0 in the present work (i.e., particle-wall contact will not be considered). The integral in Eq. 1 may be nondimensionalized and directly evaluated [33]:

$$\hat{h}_{pfw} = \frac{h_{pfw}}{k_g R_p} = 2\pi \left[(1 + \hat{\delta}) Ln \left\{ \frac{\left| \sqrt{1 - \hat{r}_{out}^2 - (1 + \hat{\delta})} \right|}{|(\hat{\delta})|} \right\} + \sqrt{1 - \hat{r}_{out}^2 - 1} \right]$$
 (2)

$$\hat{r}_{out} = \begin{cases} \sqrt{\hat{c}^2 - (1 + \hat{\delta})^2} & \hat{\delta} > \sqrt{\hat{c}^2 - 1} - 1\\ 1 & \hat{\delta} \le \sqrt{\hat{c}^2 - 1} - 1 \end{cases}$$

where \hat{C} denotes normalization by the particle radius, and $\hat{C} = R_{lens}/R_p = 1.4$ is the fluid lens proportionality constant. The rate of heat transfer at a given dimensionless separation distance $(\hat{\delta} = \delta/R_p)$ then becomes $\dot{q}_{PFW} = k_g R_p \hat{h}_{pfw}(\hat{\delta}) [T_w - T_p]$.

Numerical Techniques

Lattice Boltzmann Method (LBM)

The DNS framework is a hybrid scheme based on two coupled methods. The first is the lattice Boltzmann method (LBM), which is utilized to resolve the fluid phase - i.e., solve the Navier-Stokes (NS) equations. The LBM scheme employed here matches that developed by Ladd

and co-workers [47-49]. Due to a foundation in statistical mechanics, LBM discretizes the continuous Boltzmann equation rather than the NS equations. Since the Boltzmann equation governs the evolution of the molecular velocity distribution, LBM utilizes discrete velocity distributions (population densities) as opposed to the hydrodynamic variables. The discrete velocity distributions are updated in this work according to the classic streaming and collision process:

$$n_i(\mathbf{r} + \mathbf{c}_i \Delta t, t + \Delta t) \equiv n_i^*(\mathbf{r}, t) = n_i(\mathbf{r}, t) + \Delta_i(\mathbf{n}(\mathbf{r}, t))$$
(3)

where n_i is the discrete velocity distribution associated with molecular velocity \mathbf{c}_i , Δt is the LBM time step, Δ_i is the collision operator (function of all velocity distributions at a node, $\mathbf{n}(\mathbf{r},t)$), and n_i^* is the post-collision distribution function (expanded about the local equilibrium, \mathbf{n}^{eq}). The hydrodynamic quantities are given by the moments of the discrete distribution functions:

$$\rho = \sum_{i} n_{i} \quad \mathbf{j} = \rho \mathbf{u} = \sum_{i} n_{i} \mathbf{c}_{i} \quad \overline{\mathbf{\Pi}} = \sum_{i} n_{i} \mathbf{c}_{i} \mathbf{c}_{i}$$
 (4)

where ρ is the density, \mathbf{j} is the momentum, \mathbf{u} is the macroscopic velocity, and $\overline{\mathbf{\Pi}}$ is the fluid stress tensor. The update scheme given in Eq. 3 may ultimately be shown to recover the incompressible Navier-Stokes equations in the low Mach limit with the following closures for the shear (η) and bulk (η_b) viscosities [49]:

$$\eta = -\rho c_s^2 \left[\frac{1}{\lambda} + \frac{1}{2} \right] \qquad \eta_b = -\frac{2\rho c_s^2}{3} \left[\frac{1}{\lambda_b} + \frac{1}{2} \right] \tag{5}$$

where $c_s^2 = 1/3$ is the square of the speed of sound, and λ and λ_b are eigenvalues of the collision matrix. λ corresponds to the relaxation of the off-diagonal portion of the non-equilibrium stress tensor while λ_b corresponds to the relaxation of the diagonal portion of the non-equilibrium stress tensor. Coupling between the fluid phase and solid particles is completed by imposing a no-slip boundary condition at the particle surface. The net force and torque applied to a particle by the fluid is given by surface integration of the interphase momentum transfer (resulting from the no-slip boundary condition). While the particle in this work is held static, the force and torque may be utilized to find the new particle velocity and position (solid body mechanics). No particle collisions occur in the present work.

Random Walk Particle Tracking (RWPT)

The second method within the DNS framework is random walk particle tracking (RWPT). RWPT is employed here to solve the advection-diffusion equation for thermal energy:

$$\frac{\partial T}{\partial t} + \mathbf{u} \cdot \nabla(T) = \alpha \Delta(T) \tag{6}$$

where T is the thermal temperature and α is the thermal diffusivity. Similar to LBM, RWPT does not involve directly the continuum equation (Eq. 6 for RWPT), but instead RWPT monitors the positions of many tracers as they undergo displacement. The movement of each tracer depends

upon the local velocity field obtained via LBM as well as random fluctuations. An explicit time integration scheme is utilized within the present work to update the position of each tracer [43]:

$$\mathbf{r}_{1}(t+\Delta t) = \mathbf{r}_{1}(t) + \mathbf{u}(\mathbf{r},t)\Delta t + \xi(t) \sqrt{2\frac{\alpha_{1}^{2}}{\alpha_{2}}\Delta t} \left[1 - H\left(\zeta - \frac{\alpha_{2}}{\alpha_{1}}\right)\right]$$

$$\mathbf{r}_{2}(t+\Delta t) = \mathbf{r}_{2}(t) + \mathbf{u}(\mathbf{r},t)\Delta t + \xi(t)\sqrt{2\alpha_{2}\Delta t}$$
(7)

where \mathbf{r}_i is the position of a tracer within phase 'i', \mathbf{u} is the velocity at the tracer position before the step (found via trilinear interpolation of the LBM velocity field), $\boldsymbol{\xi}$ is a random vector whose entries are sampled from a Gaussian distribution with zero mean and unit variance, α_i is the thermal diffusivity of phase 'i', Δt is the random walk time step, H is the Heaviside function, and ζ is a random number sampled from a uniform distribution on the span [0,1] (U(0,1)). Note that an inherent assumption in Eq. 7 is that the thermal diffusivity of phase 1 is greater than phase 2 ($\alpha_1 > \alpha_2$). In the present work, α_1 will correspond to the fluid phase and α_2 will correspond to the solid particle phase. The thermal temperature in RWPT is proportional to the local tracer concentration. In the present work, we impose a temperature gradient ($\Delta T = T_1 - T_0$) by utilizing two tracer types. Tracers labeled as type '1' correspond to the higher temperature (T_1) while tracers labeled as type '0' correspond to the lower temperature (T_1). The local temperature and dimensionless temperature are given as:

$$T(\mathbf{r},t) = T_1 \frac{C_1(\mathbf{r},t)}{C_t} + T_0 \frac{C_0(\mathbf{r},t)}{C_t}$$
(8)

$$\theta(\mathbf{r},t) \equiv \frac{T(\mathbf{r},t) - T_0}{T_1 - T_0} = \frac{C_1(\mathbf{r},t)}{C_t}$$
(9)

where C_1 is the concentration of type 1 tracers, C_0 is the concentration of type 0 tracers, C_t is the total tracer concentration of tracers in the domain, and θ is the dimensionless temperature.

Systems Simulated

Uniform flow past a hot wall and a static, cold particle is considered; see Figure 2. Due to the presence of the hot wall, the steady-state fluid flow will be characterized by the development of a hydrodynamic and thermal boundary layer near the bottom plate. The center of the particle is located 5 particle diameters (D_p) away from the leading edge of the plate $(L = 5D_p)$ in all simulations, while the particle-wall separation distance (δ) and the particle Reynolds number $(Re_{Part} \equiv |U_f - U_s|D_p/v = U_\infty D_p/v)$ are varied. The range for Re_{Part} is chosen to reflect common values observed in applications concerned with wall-to-particle heat transfer [1-13] and is given by $Re_{Part} \in [1\ 10]$. The values for δ considered are chosen such that the particle resides completely within the thermal boundary layer or completely outside the thermal boundary layer and is given by $\delta/R_p \in [0.01\ 25]$. Since the distance from the leading edge (L) is fixed, the resulting plate Reynolds number $(Re_{Plate} \equiv U_\infty L/v = 5Re_{Part}; Re_{Plate} \in [5\ 50])$ lies in the intermediate regime and the flow is laminar $(Re_{Plate} < \mathcal{O}(10^6))$ [46]. The particle diameter and

Prandtl number $(Pr = v/\alpha)$ are fixed and set to $600 \, \mu m$ and 0.7, respectively. The particle diameter is resolved by 10 LBM nodes $(D_p/\Delta x_{LBM} = 10)$ in all simulations. This resolution has been shown to reach the point of grid insensitivity for uniform flow past a particle at $Re_{Part} = 40$ [24], which is well above the largest Re_{Part} considered in this work. Furthermore, test simulations were conducted at a resolution of $D_p/\Delta x_{LBM} = 20$ and the resulting heat transfer coefficients differed from the $D_p/\Delta x_{LBM} = 10$ case by less than 1%. A complete overview of the simulation conditions is given in Table 1 while the fluid and particle properties are contained within Table 2.

To impose the required boundary conditions given in Figure 2, a variety of methods were employed. The hydrodynamic boundary conditions were imposed in the LBM framework. Namely, the no-slip and uniform inflow boundary conditions were achieved via the bounce-back method [49]. The free slip and outflow boundary conditions were completed by way of the antibounce-back method [50] and extrapolation [24,51], respectively. The thermal boundary conditions were imposed in the RWPT framework. Specifically, the constant temperature boundary at the inflow ($\theta = 0.2$) and bottom wall ($\theta = 1$) was achieved by a two-step process. First, all tracers that cross the boundary are specularly reflected back into the domain. Second, a number is sampled from $\mathcal{U}(0,1)$. If the sampled value is less than or equal to θ , the tracer type is set to 1; else, the tracer type is set to 0. The inlet fluid temperature boundary condition ($\theta = 0.2$) is chosen such that it is less than the wall temperature ($\theta = 1$) but greater than the particle temperature ($\theta = 0$). By setting the inlet temperature boundary condition in this manner a thermal gradient between the particle and fluid will be sustained at large δ and the particle heat transfer will approach the Nusselt correlation for unbounded spheres. By contrast, as the particle approaches the wall ($\delta \to 0$), the inlet temperature is of less significance since the fluid near the wall will be equilibrated to the wall temperature. Therefore, the effect of the flow on wall-particle heat transfer can be directly evaluated. The constant particle temperature ($\theta = 0$) is achieved by setting all tracers that enter the particle to type 0. The adiabatic boundary is imposed by specularly reflecting tracers back into the domain (no alteration of type). The thermal outflow boundary is achieved by a semi-reflecting barrier [44]. If a tracer reaches the outflow plane, the probability of being specularly reflected back into the domain (P^*) is calculated as in [44]. A number is then sampled from $\mathcal{U}(0,1)$. If the value is less than P^* , the tracer is specularly reflected back into the domain; otherwise, the tracer is re-seeded at the inflow plane and its type is set according to the temperature boundary condition at the inflow plane ($\theta = 0.2$).

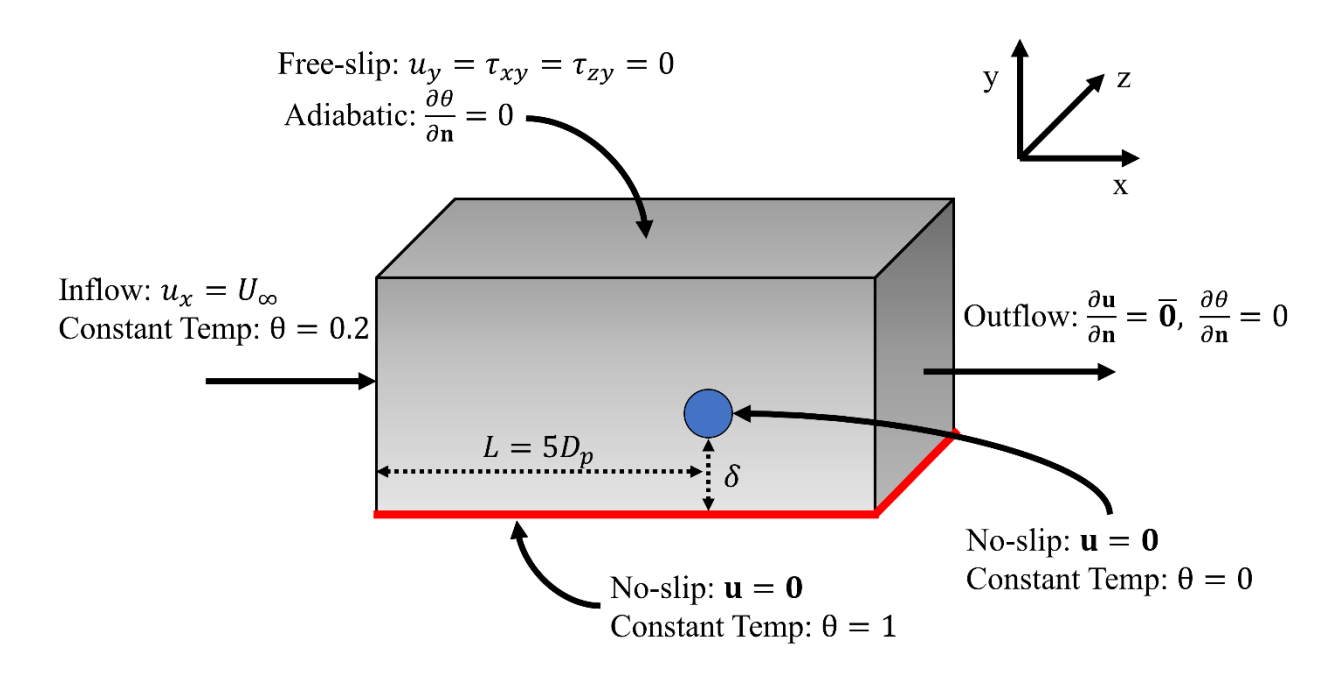


Figure 2: The geometry and boundary conditions utilized to simulate uniform flow past a hot plate (bottom wall in red) and a static, cold particle (blue sphere). The particle-wall separation distance (δ) is the distance between the bottom of the particle and the wall (varied) while L is the distance from the leading edge to the center of the particle (fixed).

Table 1. Flow Past a Hot Plate and Static, Cold Particle Simulations

Geometry and	Operating Conditions
•	

Mesh	
Nodes $(x \times y \times z)$	$160 \times 240 \times 80$
$D_p/\Delta x_{LBM}$	10
C_t	2.0
L/D_p	5

Simulation Conditions

Re_{Part}	Re_{Plate}	δ/R_p
1	5	0.01, 0.1, 0.2, 0.5, 1, 2, 4, 7, 10, 25
2	10	0.01, 0.1, 0.2, 0.5, 1, 2, 4, 7, 10, 18
4	20	0.01, 0.1, 0.2, 0.5, 1, 2, 4, 7, 10, 12
6	30	0.01, 0.1, 0.2, 0.5, 1, 2, 4, 7, 10

8	40	0.01, 0.1, 0.2, 0.5, 1, 2, 4, 7, 10
10	50	0.01, 0.1, 0.2, 0.5, 1, 2, 4, 7, 10

Table 2: Fluid and Particle Characterization

Fluid Properties

v
$$1.570 \times 10^{-5} \frac{m^2}{s^2}$$

 α_1 $2.230 \times 10^{-5} \frac{m^2}{s^2}$
 k_f $2.624 \times 10^{-2} \frac{W}{mK}$
 Pr 0.70

Particle Properties

$$D_{p}$$
 600 μm

$$\alpha_2 \qquad 8.30 \times 10^{-7} \frac{m^2}{s^2}$$

Results

In the present work, a hydrodynamic and thermal boundary layer develops near the bottom wall. From boundary layer theory, the ratio of the thermal boundary layer thickness (δ_T) to the hydrodynamic boundary layer thickness (δ_h) is found to scales as $\delta_T/\delta_h = Pr^{-1/3}$ [45-46]. For the Prandtl number considered in this work (0.7), the thermal boundary layer thickness will be larger than the hydrodynamic boundary layer thickness by approximately 12%. The extent to which the particle interacts with the thermal boundary layer depends upon the separation distance (δ); see Figures 3-4 for velocity and temperature profiles, respectively. For the case of a small separation distance (subplots (a)), the particle is within the thermal boundary layer and hence interacts with the wall more. By contrast, for large separation distances (subplots (b)), the particle is outside the thermal boundary layer (as well as the hydrodynamic boundary layer) and is less affected by the wall. Due to the thermal source at the bottom wall, a spatially varying temperature field is resulted (Figure 4).

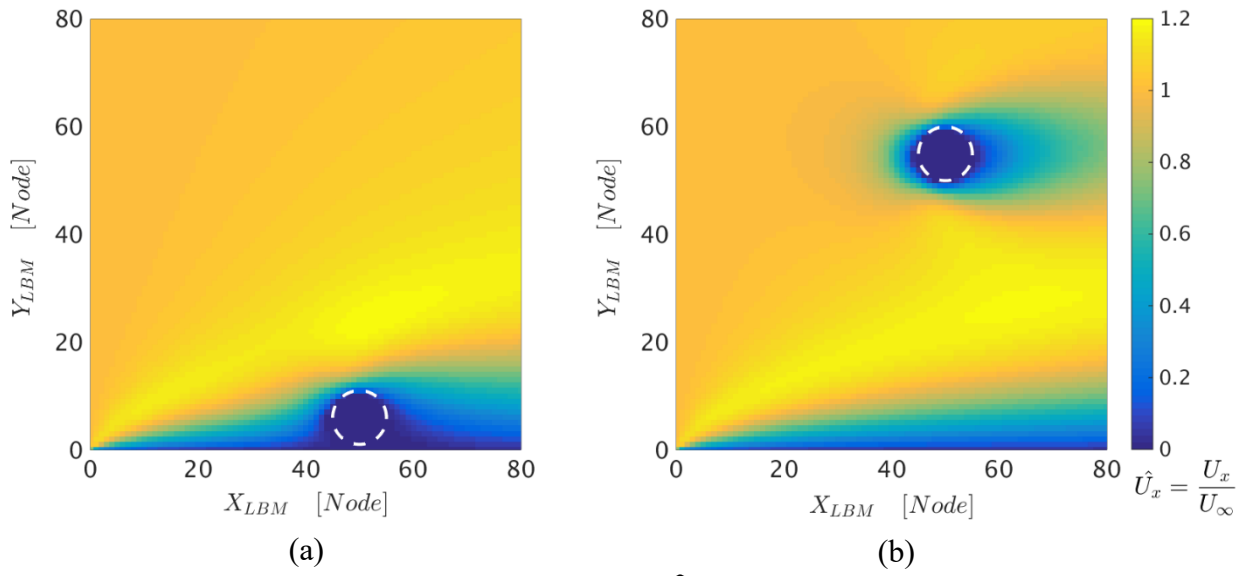


Figure 3: The dimensionless stream-wise velocity (\widehat{U}_x) profile for $Re_{Part} = 10$ and a separation distance of (a) $\delta/R_p = 0.2$ and (b) $\delta/R_p = 10.0$. The white dashed lines indicate the location of the particle.

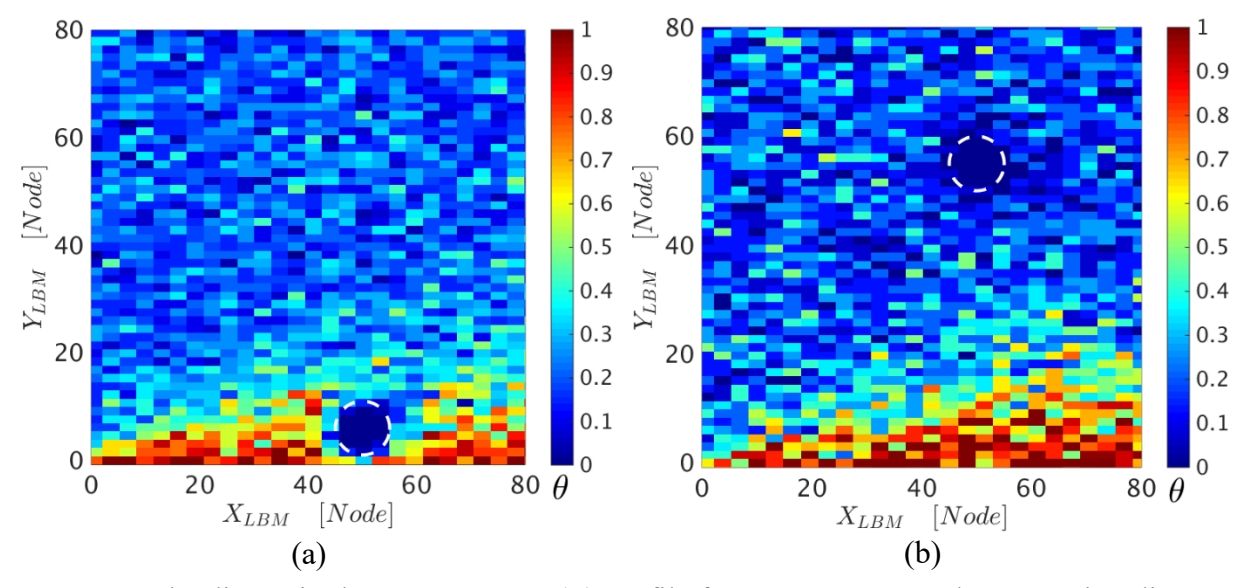


Figure 4: The dimensionless temperature (θ) profile for $Re_{Part} = 10$ and a separation distance of (a) $\delta/R_p = 0.2$ and (b) $\delta/R_p = 10.0$. The white dashed lines indicate the location of the particle.

By definition, the heat transfer coefficient (h) relates the heat flux (q) to the thermal driving force (ΔT) $(h = q)/(\Delta T)$. To quantify the heat transfer coefficient (h) or more generally the Nusselt number $(Nu = hD_p/k)$ for a particle in the near-wall region, the relevant thermal driving force (ΔT) must be defined. For the case of an unbounded system, such as in [14-17], the thermal driving force is taken to be the difference between the fluid temperature at the inflow plane $(T_{f,\infty})$ and the particle temperature (T_p) $(\Delta T = T_{f,\infty} - T_p)$. In the present work, as we are interested in the

joint influence of the incoming fluid $(T_{f,\infty})$ and the wall (T_w) , the fluid temperature surrounding the particle $(T_{f,Loc})$ is used to define the driving force. The local fluid temperature may be approximated by the integral of the fluid temperature (T_f) , with respect to a weighting function (g(r)), over a spherical volume that surrounds the particle (Ω_v) [19,25]:

$$T_{f,Loc} = \frac{\iiint g(|\mathbf{r}_y - \mathbf{r}_p|) T_f(\mathbf{r}_y) d\mathbf{\Omega}_y}{\iiint g(|\mathbf{r}_y - \mathbf{r}_p|) d\mathbf{\Omega}_y}$$
(10)

$$g(r) = \exp\left(-\frac{r}{D_p}\right), \ \frac{r}{D_p} \in [0 \ 2]$$

where $T_f(\mathbf{r}_y)$ is the fluid temperature, g(r) is the weighting function, and Ω_y is the volume contained within a sphere of radius $2D_p$ whose center coincides with the particle center (\mathbf{r}_p) . As discussed in [19], the motivation for utilizing the given form of the weighting function (g(r)) is its consistency with techniques commonly employed to derive the volume-averaged equations of motion for a gas-solids mixture [52-53]. Here, we define $\Delta T_{Loc} = T_{f,Loc} - T_p$ as the thermal driving force $(h = q''/\Delta T_{Loc})$.

Physically speaking, as δ becomes large with respect to the wall thermal boundary layer thickness (Figure 3b), the boundary effects on particle heat transfer becomes negligible and the resulting Nusselt number should converge to those obtained for an unbounded system [14-17]. However, the Nusselt numbers obtained here will not converge to [14-17], even in the limit of $\delta \to \infty$, but this is solely due to using ΔT_{Loc} instead of ΔT ; see Figure 5. The disagreement between Nu_{Loc} and existing correlations for unbounded systems [14-17] can be attributed to the interphase transfer of thermal energy that will cause $\Delta T_{Loc} < \Delta T$. For the Re_{Part} considered here, the reduction in thermal driving force ($\Delta T_{Loc} < \Delta T$) causes the resulting Nusselt numbers to be 25-50% larger than those given in [14-17]. Specifically, the Nusselt numbers obtained using $\Delta T_{Loc} = T_{f,Loc} - T_p$ (Nu_{∞}) agree with [14-17] while the Nusselt numbers obtained using $\Delta T_{Loc} = T_{f,Loc} - T_p$ (Nu_{Loc}) are larger than those given in [14-17].

In the opposite limit of separation distance $(\delta \to 0)$, a choice must be made in terms of the definition for Ω_y . Since the radius of Ω_y is $2D_p$ (significantly larger than the particle), a subset of Ω_y will overlap with the wall (Ω_w) . For this case, the volume of Ω_y overlapping with the wall (Ω_w) as well as the fluid volume (Ω_f) , was incorporated into the volume integration performed in Eq. 10 $(\Omega_y = \Omega_{f+w})$ and the temperature within Ω_w was set to the boundary condition temperature $(\theta = 1)$. This choice was motivated by the interpolation techniques employed within the DEM framework [54] to which our correlation of Nusselt number is to be applied. In DEM, the thermal driving force is found by interpolating the fluid temperature to the location of the center of the particle. If a particle lies within a numerical cell adjacent to a wall, the interpolated fluid temperature will lie between the wall temperature (T_w) and the fluid temperature at the adjacent nodes. By including Ω_w into the calculation of $T_{f,Loc}$, the resulting values are more consistent with those achieved via interpolation techniques; see Figure 6. Neglecting Ω_w and only integrating over the fluid volume $(\Omega_y = \Omega_f)$ will cause the resulting $T_{f,Loc}$ to be reduced by 16-21%, and thus the resulting heat transfer coefficients will increase. Ultimately, integration including the union between Ω_v and Ω_w was utilized in this work since it is a more conservative approach (results in

smaller predicted h values due to the larger thermal driving forces) and agrees better with interpolation of the fluid temperature.

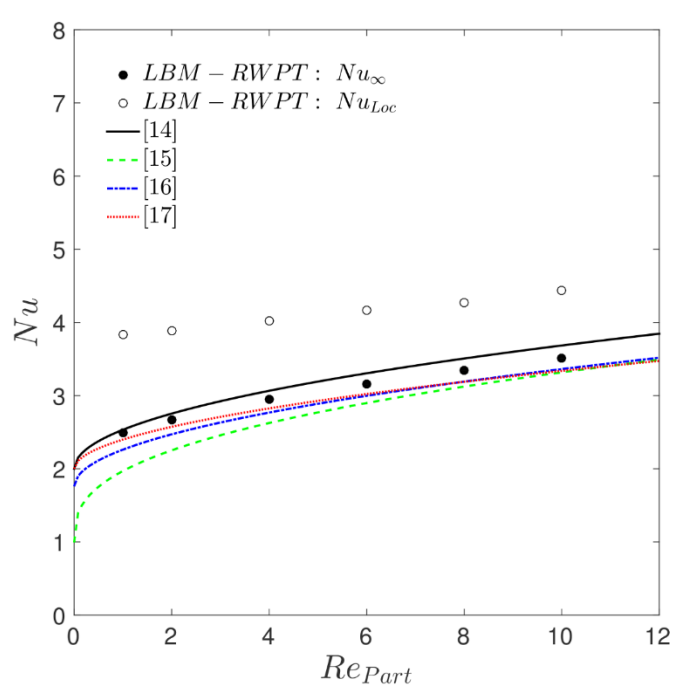


Figure 5: Comparison between the Nusselt numbers for unbounded flow past a particle when the inlet fluid temperature (Nu_{∞}) (solid black dots) versus local fluid temperature (Nu_{Loc}) (open dots) is utilized as the relevant driving force.

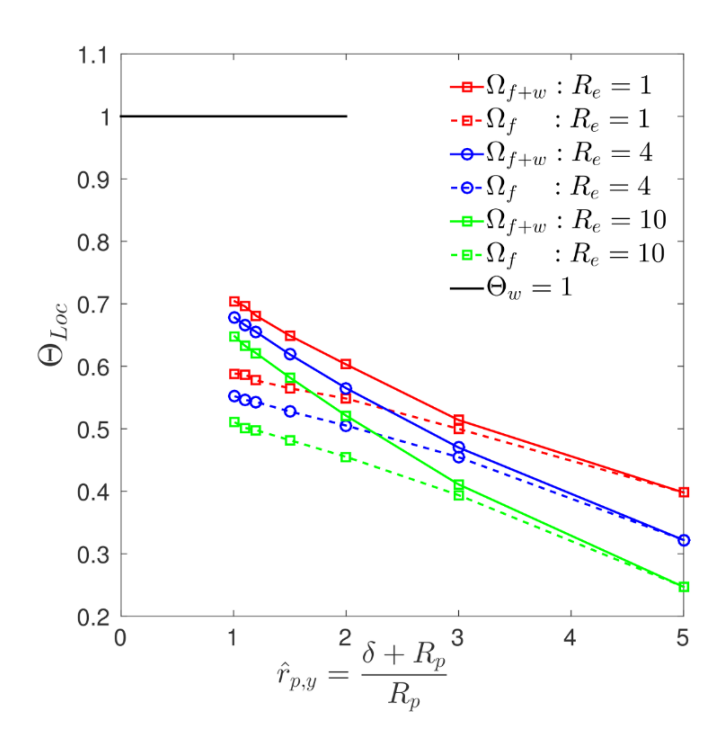


Figure 6: The local, dimensionless fluid temperature (θ_{Loc}) found via integration over Ω_y that includes wall volume (Ω_{f+w}) (solid lines) as well as just the fluid volume (Ω_f) (dashed lines) versus the dimensionless distance between the particle center and the wall $(\hat{r}_{p,y})$. Note, for $\hat{r}_{p,y} \geq 0$ does not intersect the wall $(\Omega_w = 0 \rightarrow \Omega_y = \Omega_f)$. The wall temperature (θ_w) is included for reference.

For each LBM-RWPT simulation (Table 1), the heat rate to the particle (\dot{q}) and local fluid temperature ($T_{f,Loc}$) are extracted at steady state. The heat rates obtained from LBM-RWPT (\dot{q}) are directly compared to the convective correlations (\dot{q}_{conv}) and indirect conduction theory (\dot{q}_{PFW}) commonly employed in DEM. First, the unbounded convective correlation of [14] ($\dot{q}_{conv} = h_{conv}A_p\Delta T_{Loc}$) is compared to LBM-RWPT; see Figure 7a. As the particle-wall separation distance becomes small, the heat transfer coefficient grows quite rapidly (note logarithmic x-axis) and the unbounded convection correlation fails to characterize the heat transfer enhancement that occurs in the near-wall region. This behavior is expected since the correlation given in [14] (unbounded system) does not account for the thermal source associated with the boundary. Note that the dimensionless heat rate (\hat{q}) does not decay to unity as the separation distance becomes large. This behavior is solely a result of utilizing ΔT_{Loc} as the thermal driving force (see Nu_{Loc} in Fig. 5) and \hat{q} would tend to unity if ΔT were utilized for the thermal driving force.

Inclusion of the indirect conduction mechanism [32-33] into the total heat rate $(\dot{q}_{conv} + \dot{q}_{PFW} = h_{conv}A_p\Delta T_{Loc} + k_fR_p\hat{h}_{PFW}(\hat{\delta})[T_w - T_p])$ is observed to agree markedly better with LBM-RWPT than the convection correlation alone; see Figure 7b. In contrast to the convection correlation, indirect conduction theory accounts for the effect of a boundary by assuming that one-dimensional conduction occurs through a stagnant layer of fluid between the particle and wall (R_{Lens}) . However, heat transfer enhancement due to the hot wall is still observed at length scales not predicted by indirect conduction theory (peaks in Figure 7b). The length scale for indirect conduction theory is the fluid lens thickness $(R_{Lens} - R_p)$ and is set according to the particle size $(R_{Lens} = 1.4R_p)$ [33] – i.e., \dot{q}_{PFW} only contributes to the total heat rate when $\delta < (R_{Lens} - R_p)/R_p = 0.4$ in Figure 7b.

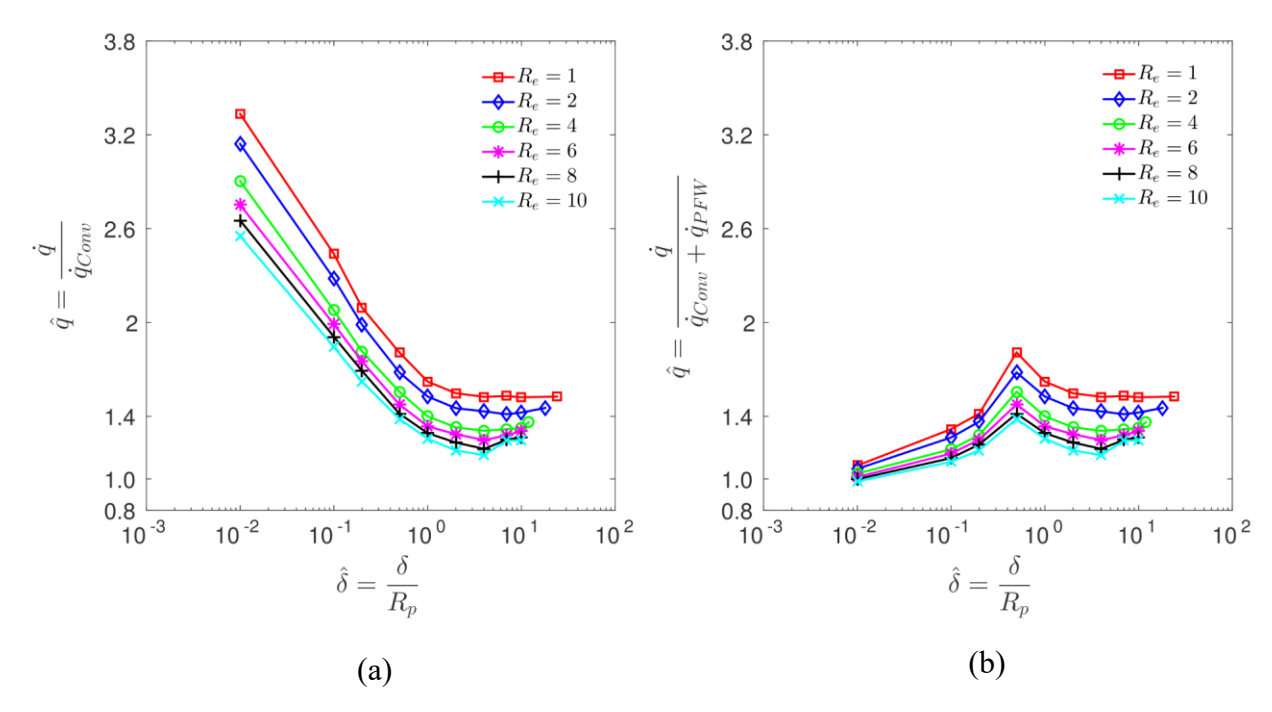


Figure 7: (a) The heat rate obtained via LBM-RWPT (\dot{q}) normalized by the correlation of [14] (\dot{q}_{conv}) and (b) the sum of [14] and indirect conduction theory [32] $(\dot{q}_{conv} + \dot{q}_{PFW})$ versus dimensionless separation distance $(\hat{\delta})$.

Physically speaking, heat transfer enhancement due to the boundary should occur at a length scale associated with the thermal boundary layer thickness (δ_T) of the plate, rather than the particle radius; see Figure 8. For example, if a particle that is large with respect to δ_T is considered (right particle in Fig. 8), the onset of indirect conduction (fluid lens just intersects the wall; $\delta =$ $0.4R_p$) would correspond to a particle outside the thermal boundary layer. For this case, the inherent assumptions of the indirect conduction theory (static, 1-D conduction) is violated since the hot fluid contained within the thermal boundary layer is advected between the particle and wall. The advection of fluid between the particle and the wall acts to reduce the thermal gradients near the particle surface from those predicted by indirect conduction theory, and thus, the heat transfer to the particle in this case is over-predicted by indirect conduction theory. By contrast, if a particle small with respect to δ_T is considered (left particle in Fig. 8), the onset of indirect conduction (fluid lens just intersects the wall; $\delta = 0.4R_p$) corresponds to a particle that is fully immersed in the boundary layer. Therefore, the heat transfer enhancement occurring when the particle is within the thermal boundary layer ($\delta < \delta_T$) but not within the fluid lens thickness ($\delta >$ $0.4R_p$) cannot be captured by indirect conduction theory - i.e., the particle may reside in the thermal boundary layer where heat transfer enhancement occurs but the fluid lens does not intersect with the wall. In this case, the heat transfer to the particle is under-predicted by indirect conduction theory. Note, that the ratio of the particle size to thermal boundary layer thickness considered in the LBM-RWPT simulations is most analogous to the 'small' case in Fig. 8, which is why the combination of convection and indirect conduction tends to under-predict the overall heat transfer (Fig. 7b).

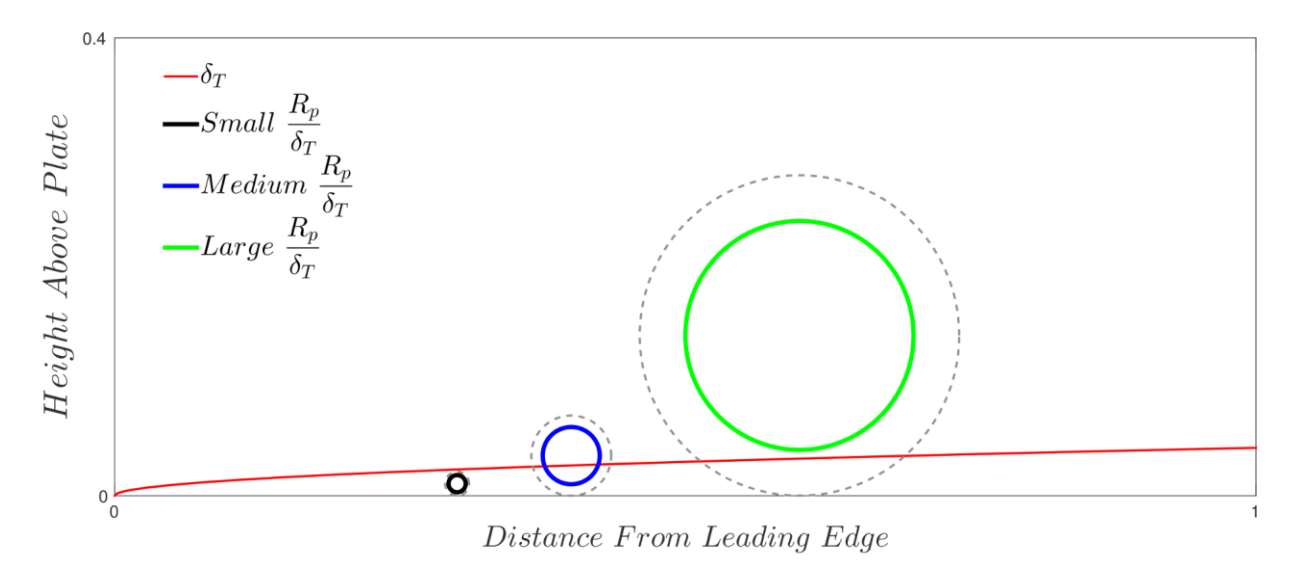


Figure 8: An illustration of particles (solid black lines) and their fluid lenses (dashed grey line) overlaid upon the scaling of the thermal boundary layer thickness (δ_T). For particles small with respect to δ_T (left particle), the onset of indirect conduction occurs when the particle is inside the boundary layer. For particles large with respect to δ_T (right particle), the onset of indirect conduction occurs when the particle is outside the boundary layer.

By taking δ_T as the relevant length scale, the heat transfer enhancement occurring in the near-wall region (Figure 7a) is more generally interpreted as the interaction between the particle and the thermal boundary layer. From classic boundary layer theory for flow past a plate, δ_T may be approximated as [45-46]:

$$\delta_T \approx 5.0 \frac{\chi}{Re_{Plate}^{1/2}} Pr^{-1/3} \tag{11}$$

where x is the distance from the leading edge $(5D_p$ in this work). The local Nusselt number $(Nu_{Loc} = hD_p/k; h = q^{"}/\Delta T_{Loc})$ for the unbounded system (open dots in Figure 5) may be approximated by the following fit

$$Nu_{Loc} = 3.75 + 0.0675Re_{Part}. (12)$$

By utilizing δ_T as the relevant length scale and Nu_{Loc} as the asymptotic limit for large particle-wall separation distances ($\delta \to \infty$), a compression of the LBM-RWPT data may be completed; see Figure 9. The data in Figure 9 is approximated by:

$$f_1(\hat{\delta}) = 1 + 0.8 \exp(-260\hat{\delta}) + 0.53 \exp(-35\hat{\delta}) - 0.002 \exp(-0.5\hat{\delta}), \text{ or}$$
 (13)
 $f_2(\hat{\delta}) = 1 + 1.13 \exp(-85\hat{\delta})$

where $\hat{\delta} = \delta/\delta_T$ is the dimensionless separation distance. Making use of Eqs. 12-13, the Nusselt number in the near-wall region then becomes

$$Nu \equiv \frac{hD_p}{k_f} = f_i(\hat{\delta}) Nu_{Loc}$$
 (14)

where $f_i(\hat{\delta})$ is either $f_1(\hat{\delta})$ or $f_2(\hat{\delta})$ in Eq. 13. Since the heat transfer enhancement in the nearwall region grows rapidly as the separation distance becomes small $(\hat{\delta} \to 0 \text{ in Fig. 9})$, the accuracy of the fitting function $(f_i(\hat{\delta}))$ is better illustrated on a log axis. Due to the larger number of fitting parameters, f_1 better characterizes the data. However, very reasonable accuracy is obtained with the reduced order f_2 function. Note that both f_1 and f_2 asymptotically decay to unity as $\hat{\delta} \to \infty$, which is the physically correct behavior $(Nu \to Nu_{Loc})$. The choice between f_1 and f_2 should be dictated by the desired accuracy. Therefore, the Nusselt correlation given by Eq. 14 seams together the unbounded and near-wall region while accounting for both convective and indirect conduction mechanisms. While the $f_i(\hat{\delta})$ fitting functions monotonically decay with increasing $\hat{\delta}$, the LBM-RWPT data displays a local minimum at $\hat{\delta} \approx 0.5$ that becomes more pronounced with increasing Re_{Part} . As Re_{Part} increases, the thermal and flow length scales compress. By contrast, the volume element utilized to calculate T_{Loc} remains constant (sphere of radius $2D_p$ in Eq. 10). Therefore, the spatial averaging in Eq. 10 begins to encompass regions of the hot boundary layer that are not significantly contributing to the particle heat transfer - i.e., T_{Loc} is increased by averaging over hot fluid near the bottom wall that will tend to be advected away as Re_{Part} increases.

Due to the restrictions on parameter space, the formal accuracy of indirect conduction theory for a generic system is outside of the scope of the present work. However, by identifying the thermal boundary layer thickness as the key length scale, some general trends may be noted. For particles that are large with respect to δ_T (right particle in Fig. 8), the current indirect conduction theories within DEM are expected to over-predict the heat transfer to the particle. This can be traced back to the violation of the static-fluid lens assumption over a length scale of $0.4R_p$. Note that the boundary layer thickness can vary spatially and will compress with increasing Reynolds and Prandtl number. For the case of a particle that is small with respect to δ_T (left particle in Fig. 8), the current indirect conduction theories are expected to under-predict the heat transfer to the particle (observed here in Fig. 7b). In this case, the particle is well within the boundary layer (where heat transfer enhancement occurs) at the onset of indirect conduction ($\delta \leq 0.4R_p$).

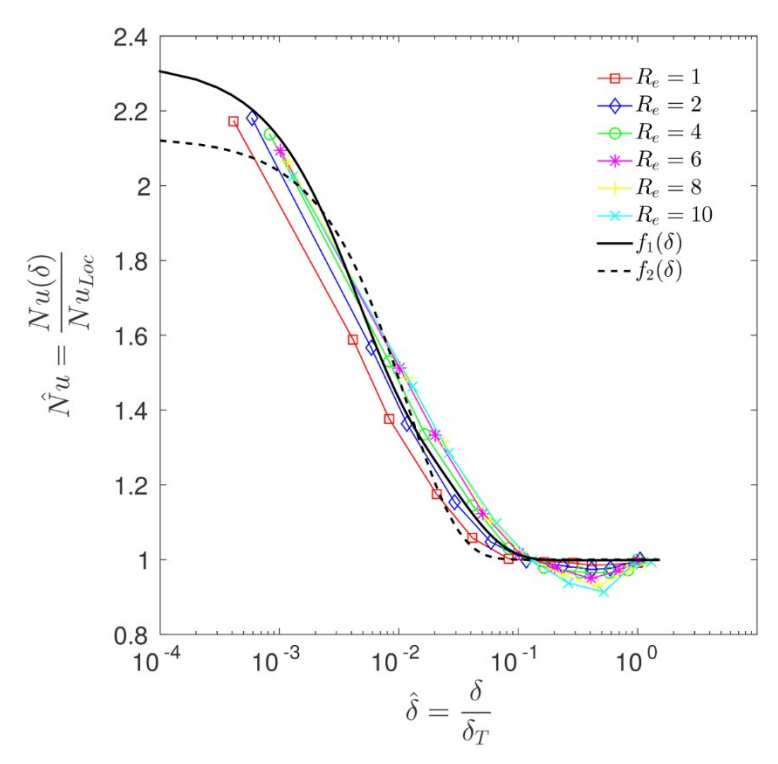


Figure 9: The Nusselt number obtained via LBM-RWPT normalized by the local Nusselt number (open dots in Figure 5) versus the non-dimensional separation distance on a logarithmic axis.

Conclusions

Direct numerical simulation (DNS) was utilized to examine the effect of a hot boundary on heat transfer to a solid particle in a laminar, thermal boundary layer. The heat rate obtained via LBM-RWPT shows that Nusselt correlations developed in unbounded systems (no walls) are not sufficient in the near-wall region while the combination of such correlations with indirect conduction theory agrees markedly better with DNS. Nonetheless, such modified correlations still exhibit discrepancies with DNS that can be traced to thermal and hydrodynamic length scales of the system.

More specifically, the length scale associated with near-wall heat transfer enhancement is found to be proportional to the thermal boundary layer thickness and not the particle radius, as is utilized by indirect conduction theory. Furthermore, the use of the local fluid temperature (as opposed to the free stream temperature) increases the universality of the resulting Nusselt numbers since it accounts for the effects of all the boundary conditions. However, the local fluid temperature is not known a priori and must instead be computed on the fly. The thermal boundary layer thickness and local Nusselt number (unbounded system with local fluid temperature as the driving force) are utilized to compress the LBM-RWPT data and develop a new correlation which is valid in the near-wall region. The new correlation asymptotically decays to the unbounded convection correlation in the limit of large particle-wall separation distance, and thus seams together the unbounded and near-wall regions.

While not considered here, the particle(s) may translate in space as well as rotate (angular velocity). Furthermore, the diameter of the particle, distance from the leading edge, Prandtl

number, and thermal wall boundary condition may be altered. The impact of each parameter on particle heat transfer is not known a priori but will be the subject of future work - i.e., testing the robustness of the present relation for Nu.

Acknowledgements

The authors gratefully acknowledge funding support provided by the National Science Foundation under Grant CBET 1512630.

Literature Cited

- [1] Ansart, R., García-Triñanes, P., Boissière, B., Benoit, H., P.K. Seville, J., Simonin, O., 2017. Dense gas-particle suspension upward flow used as heat transfer fluid in solar receiver: PEPT experiments and 3D numerical simulations. Powder Technology 307, 25–36. https://doi.org/10.1016/j.powtec.2016.11.006
- [2] Bongo Njeng, A.S., Vitu, S., Clausse, M., Dirion, J.-L., Debacq, M., 2018. Wall-to-solid heat transfer coefficient in flighted rotary kilns: Experimental determination and modeling. Experimental Thermal and Fluid Science 91, 197–213. https://doi.org/10.1016/j.expthermflusci.2017.10.024
- [3] Chaudhuri, B., Muzzio, F.J., Tomassone, M.S., 2006. Modeling of heat transfer in granular flow in rotating vessels. Chemical Engineering Science 61, 6348–6360. https://doi.org/10.1016/j.ces.2006.05.034
- [4] Cong, T.N., He, Y., Chen, H., Ding, Y., Wen, D., 2007. Heat transfer of gas—solid two-phase mixtures flowing through a packed bed under constant wall heat flux conditions. Chemical Engineering Journal 130, 1–10. https://doi.org/10.1016/j.cej.2006.11.006
- [5] Kuipers, J. a. M., Prins, W., Van Swaaij, W.P.M., 1992. Numerical calculation of wall-to-bed heat-transfer coefficients in gas-fluidized beds. AIChE J. 38, 1079–1091. https://doi.org/10.1002/aic.690380711
- [6] Martinek, J., Ma, Z., 2014. Granular Flow and Heat Transfer Study in a Near-Blackbody Enclosed Particle Receiver V001T02A012. https://doi.org/10.1115/ES2014-6393
- [7] Morris, A.B., Ma, Z., Pannala, S., Hrenya, C.M., 2016. Simulations of heat transfer to solid particles flowing through an array of heated tubes. Solar Energy 130, 101–115. https://doi.org/10.1016/j.solener.2016.01.033
- [8] Morris, A.B., Pannala, S., Ma, Z., Hrenya, C.M., 2015. A conductive heat transfer model for particle flows over immersed surfaces. International Journal of Heat and Mass Transfer 89, 1277–1289. https://doi.org/10.1016/j.ijheatmasstransfer.2015.06.004
- [9] Nijemeisland, M., Dixon, A.G., 2004. CFD study of fluid flow and wall heat transfer in a fixed bed of spheres. AIChE J. 50, 906–921. https://doi.org/10.1002/aic.10089
- [10] Patil D. J., Smit J., van Sint Annaland M., Kuipers J. A. M., 2005. Wall-to-bed heat transfer in gas—solid bubbling fluidized beds. AIChE Journal 52, 58–74. https://doi.org/10.1002/aic.10590
- [11] Shi, D., Vargas, W.L., McCarthy, J.J., 2008. Heat transfer in rotary kilns with interstitial gases. Chemical Engineering Science 63, 4506–4516. https://doi.org/10.1016/j.ces.2008.06.006
- [12] Syamlal, M., Gidaspow, D., 1985. Hydrodynamics of fluidization prediction of wall to bed heat-transfer coefficients. AIChE Journal 31, 127–135.
- [13] Yohannes, B., Emady, H., Anderson, K., Paredes, I., Javed, M., Borghard, W., Muzzio, F.J., Glasser, B.J., Cuitiño, A.M., 2016. Scaling of heat transfer and temperature distribution in granular flows in rotating drums. Phys. Rev. E 94, 042902. https://doi.org/10.1103/PhysRevE.94.042902
- [14] Ranz, W.E., Marshall, W.R., 1952. Evaporation from drops. Chem. Eng. Prog. 48, 141.
- [15] Feng, Z.-G., Michaelides, E.E., 2000. A numerical study on the transient heat transfer from a sphere at high Reynolds and Peclet numbers. International Journal of Heat and Mass Transfer 43, 219–229. https://doi.org/10.1016/S0017-9310(99)00133-7
- [16] Richter, A., Nikrityuk, P.A., 2012. Drag forces and heat transfer coefficients for spherical, cuboidal and ellipsoidal particles in cross flow at sub-critical Reynolds numbers.

- International Journal of Heat and Mass Transfer 55, 1343–1354. https://doi.org/10.1016/j.ijheatmasstransfer.2011.09.005
- [17] Whitaker, S., 1972. Forced convection heat transfer correlations for flow in pipes, past flat plates, single cylinders, single spheres, and for flow in packed beds and tube bundles. AIChE J. 18, 361–371. https://doi.org/10.1002/aic.690180219
- [18] Dan, C., Wachs, A., 2010. Direct Numerical Simulation of particulate flow with heat transfer. International Journal of Heat and Fluid Flow, 7th World Conference on Experimental Heat Transfer, Fluid Mechanics and Thermodynamics (ExHFT-7), Krakow and The Conference on Modelling Fluid Flow (CMFF '09), Budapest 31, 1050–1057. https://doi.org/10.1016/j.ijheatfluidflow.2010.07.007
- [19] Deen, N.G., Kriebitzsch, S.H.L., van der Hoef, M.A., Kuipers, J.A.M., 2012. Direct numerical simulation of flow and heat transfer in dense fluid–particle systems. Chemical Engineering Science 81, 329–344. https://doi.org/10.1016/j.ces.2012.06.055
- [20] Deen, N.G., Peters, E.A.J.F., Padding, J.T., Kuipers, J.A.M., 2014. Review of direct numerical simulation of fluid–particle mass, momentum and heat transfer in dense gas—solid flows. Chemical Engineering Science 116, 710–724. https://doi.org/10.1016/j.ces.2014.05.039
- [21] Feng, Z.-G., Michaelides, E.E., 2009. Heat transfer in particulate flows with Direct Numerical Simulation (DNS). International Journal of Heat and Mass Transfer 52, 777–786. https://doi.org/10.1016/j.ijheatmasstransfer.2008.07.023
- [22] Feng, Z.-G., Michaelides, E.E., 2008. Inclusion of heat transfer computations for particle laden flows. Physics of Fluids 20, 040604. https://doi.org/10.1063/1.2911022
- [23] Kravets, B., Kruggel-Emden, H., 2017. Investigation of local heat transfer in random particle packings by a fully resolved LBM-approach. Powder Technology 318, 293–305. https://doi.org/10.1016/j.powtec.2017.05.039
- [24] Kruggel-Emden, H., Kravets, B., Suryanarayana, M.K., Jasevicius, R., 2016. Direct numerical simulation of coupled fluid flow and heat transfer for single particles and particle packings by a LBM-approach. Powder Technology 294, 236–251. https://doi.org/10.1016/j.powtec.2016.02.038
- [25] Tavassoli, H., Kriebitzsch, S.H.L., van der Hoef, M.A., Peters, E.A.J.F., Kuipers, J.A.M., 2013. Direct numerical simulation of particulate flow with heat transfer. International Journal of Multiphase Flow 57, 29–37. https://doi.org/10.1016/j.ijmultiphaseflow.2013.06.009
- [26] Tavassoli, H., Peters, E.A.J.F., Kuipers, J.A.M., 2015. Direct numerical simulation of fluid–particle heat transfer in fixed random arrays of non-spherical particles. Chemical Engineering Science 129, 42–48. https://doi.org/10.1016/j.ces.2015.02.024
- [27] Radl, S., Municchi, F., Goniva, C., 2016. APS -69th Annual Meeting of the APS Division of Fluid Dynamics Event Near-wall effects for momentum, heat and mass transport in gas-particle suspensions at moderate Reynolds numbers, in: Bulletin of the American Physical Society. Presented at the 69th Annual Meeting of the APS Division of Fluid Dynamics, American Physical Society.
- [28] Flamant G, Menigault T. Combined wall-to-fluidized bed heat transfer. Bubbles and emulsion contributions at high temperature. International Journal of Heat and Mass Transfer. 1987;30(9):1803-1812. doi:10.1016/0017-9310(87)90239-0.
- [29] Wen C, Chang T. Particle to particle heat transfer in air fluidized beds. Proceedings of international symposium on fluidization, Eindhoven. 1967:491-506.

- [30] Batchelor, G.K., O'Brien, R.W., 1977. Thermal or electrical conduction through a granular material. Proceedings of the Royal Society of London A: Mathematical, Physical and Engineering Sciences 355, 313–333. https://doi.org/10.1098/rspa.1977.0100
- [31] Cooper, M.G., Mikic, B.B., Yovanovich, M.M., 1969. Thermal contact conductance. International Journal of Heat and Mass Transfer 12, 279–300. https://doi.org/10.1016/0017-9310(69)90011-8
- [32] Rong, D., Horio, M., 1999. DEM simulation of char combustion in a fluidized bed. Second International Conference on CFD in the Minerals and Process Industries CSIRO 65–70.
- [33] Lattanzi Aaron M., Hrenya Christine M., 2017. Indirect conduction in gas–solids systems: Static vs. Dynamic effects. AIChE Journal 63, 4685–4693. https://doi.org/10.1002/aic.15802
- [34] Vargas WL, McCarthy JJ. Conductivity of granular media with stagnant interstitial fluids via thermal particle dynamics simulation. International Journal of Heat and Mass Transfer. 2002;45(24):4847-4856. doi:10.1016/S0017-9310(02)00175-8.
- [35] Cheng GJ, Yu AB, Zulli P. Evaluation of effective thermal conductivity from the structure of a packed bed. Chemical Engineering Science. 1999;54(19):4199-4209. doi:10.1016/S0009-2509(99)00125-6.
- [36] Delvosalle C, Vanderschuren J. Gas-to-particle and particle-to-particle heat transfer in fluidized beds of large particles. Chemical Engineering Science. 1985;40(5):769-779. doi:10.1016/0009-2509(85)85030-2.
- [37] Lattanzi, A.M., Hrenya, C.M., 2016. A coupled, multiphase heat flux boundary condition for the discrete element method. Chemical Engineering Journal 304, 766–773. https://doi.org/10.1016/j.cej.2016.07.004
- [38] Di Maio FP, Di Renzo A, Trevisan D. Comparison of heat transfer models in DEM-CFD simulations of fluidized beds with an immersed probe. Powder Technology. 2009;193(3):257-265. doi:10.1016/j.powtec.2009.03.002.
- [39] Zhou ZY, Yu AB, Zulli P. Particle scale study of heat transfer in packed and bubbling fluidized beds. AIChE J. 2009;55(4):868-884. doi:10.1002/aic.11823.
- [40] Zhou H, Flamant G, Gauthier D. DEM-LES simulation of coal combustion in a bubbling fluidized bed Part II: coal combustion at the particle level. Chemical Engineering Science. 2004;59(20):4205-4215. doi:10.1016/j.ces.2004.01.070.
- [41] Metzger, B., Rahli, O., Yin, X., 2013. Heat transfer across sheared suspensions: role of the shear-induced diffusion. Journal of Fluid Mechanics 724, 527–552. https://doi.org/10.1017/jfm.2013.173
- [42] Wang, L., Koch, D., Yin, X., Cohen, C., 2009. Hydrodynamic diffusion and mass transfer across a sheared suspension of neutrally buoyant spheres. Physics of Fluids 21, 033303. https://doi.org/10.1063/1.3098446
- [43] Lattanzi, A.M., Yin X., and Hrenya C.M., 2018. A Hybrid Lattice Boltzmann Random Walk Method for Heat Transfer in Gas-Solids Systems. Journal of Computational Physics, *Submitted*.
- [44] Lattanzi, A.M., Yin X., and Hrenya C.M., 2018. An Outflow Boundary Condition for the Random Walk Particle Tracking Method. International Journal of Heat and Mass Transfer, *Submitted*.
- [45] Schlichting, H., Gersten, K., 2000. Boundary-Layer Theory, 8th edition. ed. Springer, Berlin; New York.
- [46] White, F., 1991. Viscous Fluid Flow, 2nd ed. McGraw-Hill, New York, NY.

- [47] Ladd, A.J.C., 1994a. Numerical simulations of particulate suspensions via a discretized Boltzmann equation. Part 1. Theoretical foundation. Journal of Fluid Mechanics 271, 285–309. https://doi.org/10.1017/S0022112094001771
- [48] Ladd, A.J.C., 1994b. Numerical simulations of particulate suspensions via a discretized Boltzmann equation. Part 2. Numerical results. Journal of Fluid Mechanics 271, 311–339. https://doi.org/10.1017/S0022112094001783
- [49] Ladd, A.J.C., Verberg, R., 2001. Lattice-Boltzmann Simulations of Particle-Fluid Suspensions. Journal of Statistical Physics 104, 1191–1251. https://doi.org/10.1023/A:1010414013942
- [50] Janßen, C., Krafczyk, M., 2011. Free surface flow simulations on GPGPUs using the LBM. Computers & Mathematics with Applications, Mesoscopic Methods for Engineering and Science Proceedings of ICMMES-09Mesoscopic Methods for Engineering and Science 61, 3549–3563. https://doi.org/10.1016/j.camwa.2011.03.016
- [51] Yang, Z., 2013. Lattice Boltzmann outflow treatments: Convective conditions and others. Computers & Mathematics with Applications, Special Issue on Mesoscopic Methods in Engineering and Science (ICMMES-2010, Edmonton, Canada) 65, 160–171. https://doi.org/10.1016/j.camwa.2012.11.012
- [52] Anderson, T.B., Jackson, R., 1967. Fluid mechanical description of fluidized beds. equations of motion. Ind. Eng. Chem. Fund. 6, 527–539. https://doi.org/10.1021/i160024a007
- [53] Jackson, R., 1997. Locally averaged equations of motion for a mixture of identical spherical particles and a Newtonian fluid. Chemical Engineering Science, Mathematical modelling of chemical and biochemical processes 52, 2457–2469. https://doi.org/10.1016/S0009-2509(97)00065-1
- [54] Garg, R., Galvin, J., Li, T., 2012. Documentation of open-source MFIX–DEM software for gas-solids flows 40. https://mfix.netl.doe.gov/documentation/dem doc 2012-1.pdf